Photocatalysis

DOI: 10.1002/anie.201407319

Helical Graphitic Carbon Nitrides with Photocatalytic and Optical Activities**

*Yun Zheng, Lihua Lin, Xiangju Ye, Fangsong Guo, and Xinchen Wang**

Abstract: *Graphitic carbon nitride can be imprinted with a twisted hexagonal rod-like morphology by a nanocasting technique using chiral silicon dioxides as templates. The helical nanoarchitectures promote charge separation and mass transfer of carbon nitride semiconductors, enabling it to act as a more efficient photocatalyst for water splitting and CO_2 reduction than the pristine carbon nitride polymer. This is to our knowledge a unique example of chiral graphitic carbon nitride that features both left- and right-handed helical nanostructures and exhibits unique optical activity to circularly polarized light at the semiconductor absorption edge as well as photoredox activity for solar-to-chemical conversion. Such helical nanostructured polymeric semiconductors are envisaged to hold great promise for a range of applications that rely on such semiconductor properties as well as chirality for photocatalysis, asymmetric catalysis, chiral recognition, nanotechnology, and chemical sensing.*

The helix is one of the most fascinating structures in nature. Helical conformation is widespread from biomolecules (amino acids and sugars) to biomacromolecules (DNA, RNA, and proteins), microorganisms (helix-shaped viruses), and macroscopic living systems (vines, timbo, and snails).[1] Concurrently to the study of naturally occurring substances, the synthesis of helical nanostructured materials has become one of the hot issues nowadays. The design of helical nanostructures in polymers,[2] carbonaceous materials,[3] and metal oxides (e.g. ZnO, TiO_2, and SiO_2)[4] has recently gained considerable attention. Such helical nanostructured materials are attractive because they exhibit optimized morphology and texture as well as unique chirality and optical activity,[5] which might have potential applications in the fields of optical devices, chiral recognition, asymmetric catalysis, and photosynthesis.

[*] Y. Zheng, L. Lin, X. Ye, F. Guo, Prof. X. Wang
State Key Laboratory of Photocatalysis on Energy and Environment
College of Chemistry, Fuzhou University
Fuzhou 350002 (China)
E-mail: xcwang@fzu.edu.cn
Homepage: http://wanglab.fzu.edu.cn

[**] Supported by the National Basic Research Program of China (2013CB632405), the National Natural Science Foundation of China (21033003 and 21173043), the State Key Laboratory of NBC Protection for Civilian (SKLNBC2013-04K), the Specialized Research Fund for the Doctoral Program of Higher Education (20133514110003), and the Department of Education of Fujian Province in China. X. Wang thanks the support of The National Science Fund for Distinguished Young Scholars.

Supporting information for this article is available on the WWW under http://dx.doi.org/10.1002/anie.201407319.

Artificial photosynthesis is a strategy to capture and store the energy from sunlight in the chemical bonds of fuels, such as hydrogen and hydrocarbons.[6] Melon-based graphitic carbon nitride polymer (termed as g-C_3N_4 for simplicity), which consists of two-dimensional (2D) conjugated planes packed together with tri-*s*-triazine repeating units through van der Waals interactions, has recently emerged as a metal-free polymeric photocatalyst for various relevant chemical reactions, including water splitting,[7] CO_2 reduction,[8] phenol synthesis from benzene,[9] and the selective oxidation of aromatic alcohols.[10] Recently, nanostructured g-C_3N_4 has attracted ever-growing interest in the field of catalysis, photocatalysis, chemical sensors, and biological imaging, because nanostructure engineering is an efficient protocol to tailor the morphology, texture, electronic structure, optical and surface properties as well as the photocatalytic function of g-C_3N_4. To date, various nanoarchitectural g-C_3N_4, ranging from one-dimensional nanorods and nanowires, to two-dimensional nanosheets, and three-dimensional mesoporous structures, have been prepared by many approaches, such as hard/soft template synthesis,[11] sulfur mediated synthesis,[12] solvothermal/molten-salt technology,[13] exfoliation methods,[14a–c] and supramolecular chemistry.[14d,e] More recently, Antonietti and co-workers reported that uniform g-C_3N_4 nanorods can be obtained by a hard-templating method using chiral mesostructured silica nanorods, and these g-C_3N_4 nanorods showed photocatalytic activity,[15] albeit accurate chiral (instead of morphological) translation from the silica to g-C_3N_4 semiconductor has yet to be reported. Thus far, we notice that there is no description available on the organization of the 2D g-C_3N_4 semiconductor into helical nanostructures with photocatalytic and optical activities.

Herein, we demonstrated that g-C_3N_4 with a helical rod-like morphology (HR-CN) is synthesized by a nanocasting approach using chiral mesoporous silica (CMS) as the sacrificial template. CMS, which features a helical hexagonal rod-like morphology and ordered channels winding around the central axis of the rods, enables the construction of twisted nanoarchitectures by directing the assembly of the building blocks.[16] The infiltration of the cyanamide (CY) precursor into the CMS template is the vital step in the preparation of HR-CN. As shown in Scheme 1, CMS is acidified with HCl (1M) to promote the affinity between CMS and cyanamide through acid–base interaction. Then, a technique of sonication under vacuum is exploited to pump CY molecules into the pores/channels of CMS. The obtained CMS/CY mixture is subjected to a thermal polymerization under N_2 atmosphere to generate CMS/g-C_3N_4. Finally, after being etched by NH_4HF_2 solution and washed with water and ethanol, the silica template is completely removed and the resultant HR-

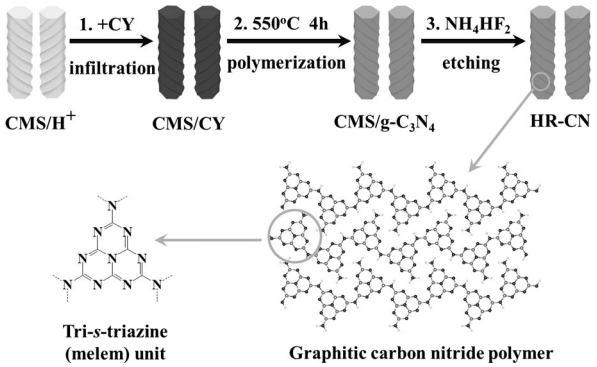

Scheme 1. Synthetic process for helical nanorod-like graphitic carbon nitride (HR-CN) based on chiral mesoporous silica (CMS) as the template and cyanamide (CY) as the precursor.

CN sample is obtained. As a reference sample, bulk g-C_3N_4 (B-CN) was also synthesized by heating CY with the same thermal treatment procedure as the HR-CN synthesis.

The surface morphology of HR-CN is characterized by scanning emission microscopy (SEM) and transmission electron microscopy (TEM) images. The SEM images (Figures 1 and S3) show that HR-CN exhibits uniform and monodisperse twisted hexagonal rod-like morphology, ca. 100–200 nm in outer diameter and 0.5–2.0 μm in length. The similar morphology between HR-CN and CMS (Figure S2) confirms that the helical nanoarchitecture and geometrical feature of HR-CN are precisely replicated from the template of CMS. HR-CN consists of both, left-handed and right-handed nanorods (Figure S1), and the left/right handedness ratio was > 1:1 by counting the characteristic morphologies from 500 randomly chosen nanohelices in the SEM images. Choosing a typical rod for TEM and HRTEM analysis (Figures 1b and S3), we can see a spiral rod with a length of 1.6 μm and a diameter of 130 nm. The enlarged surface and edge of the nanorod provides the clue that the nanorod is composed of layered carbon nitride sheets as building blocks.[15] Additionally, it should be noted that the nanorod of HR-CN is a stuffed one rather than a hollow one. The TEM-EDX spectra further identify the existence of two major elements (C, N) in the selected nanorod of HR-CN (Figure S5a). As confirmed by thermogravimetric analysis (TGA) (Figure S6a), less than 1% silica residues were found in the final HR-CN sample,

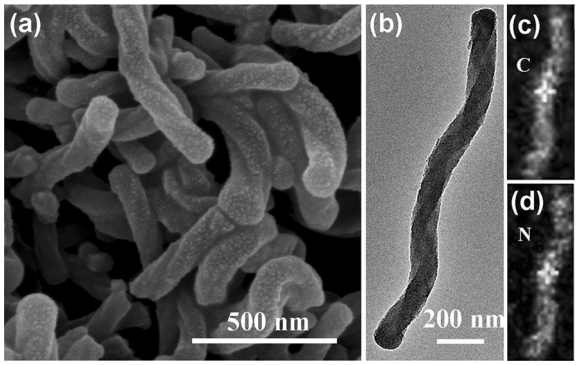

Figure 1. Morphology characterization of the HR-CN sample. a) SEM, b) TEM, and c,d) corresponding elemental mapping images of C, N for HR-CN.

indicating that most of the silica was successfully removed after the etching operation. The mapping images (Figure 1c and d) show that both C and N elements are homogeneously distributed in a spiral way similar to the shape of the selected helical nanorod.

The textures of HR-CN were analyzed by N_2-sorption measurements (Figure S4). For the CMS template, a type IV feature with a capillary condensation step at 0.4 in relative pressure demonstrates the existence of the mesoporous structure. Although CMS has a large specific surface area (489 $m^2 g^{-1}$) and uniform mesopores (ca. 3.3 nm in size), the texture of HR-CN is quite different. Firstly, the specific surface area of HR-CN is ca. 56 $m^2 g^{-1}$, which is smaller than that of CMS, but still much larger than that of B-CN (ca. 4 $m^2 g^{-1}$). Secondly, the Barrett–Joyner–Halenda (BJH) adsorption pore size distribution of HR-CN shows two types of pores, i.e., small mesopores (ca. 3.8 nm) and large complementary mesopores (ca. 10.7 nm). The mechanism of the generation of two types of pores has been demonstrated in a mesoporous carbon nitride.[17]

As measured by elemental analysis, the C/N molar ratio of HR-CN and B-CN were ca. 0.70 and 0.68, respectively, and both of them are close to the theoretical value of idealized g-C_3N_4 (0.75). This indicates the successful formation of the polymeric framework from the CY precursor.[7a,18] The XRD peak of HR-CN (Figure 2a) at 13.0° is due to the in-plane repeating motifs of the continuous heptazine frameworks, whereas the peak at 27.4° corresponds to the (002) reflection of a graphitic structure with a *d*-value of 0.326 nm.[19] However, a broader XRD reflection with a lower intensity is observed for HR-CN, because the helical nanostructure can reduce the correlation length of interlayer periodicity of tri-*s*-triazine building blocks. In the FTIR spectrum of HR-CN (Figure 2b), the bands at 3100 cm^{-1}, 1200–1600 cm^{-1}, and 810 cm^{-1} belong to primary and secondary amines, aromatic carbon and nitrogen heterocycles, and the *s*-triazine ring, respectively.[7a,19a] The solid-state ^{13}C NMR spectrum (Figure S6b) confirms the existence of heptazine units in HR-CN, and the response at ca. 164.3 and 155.6 ppm was assigned to a poly(tri-*s*-triazine) structure. The first peak is ascribed to the C(e) atoms [$CN_2(NH_x)$], whereas the second one is attributed to the C(i) atoms of melem (CN_3).[19b,20] Since nearly all the XRD, FTIR, and ^{13}C NMR spectra of the HR-CN sample resemble those of the B-CN reference, a graphitic-like structure composed of heptazine heterocyclic rings exists in HR-CN and remains almost unchanged after helical engineering and NH_4HF_2 etching.

The optical absorption and energy band gap are greatly altered after the introduction of the helical structure, as apparent from the UV/Vis diffuse reflectance spectroscopy (DRS) measurements (Figures 4 and S6c). An improved light-harvesting capability across the whole optical spectrum, especially at wavelengths exceeding 420 nm, is found for HR-CN, mainly owing to the multiple reflections of incident light.[20b,21] In comparison with B-CN, a slight hypsochromic shift of the photoabsorption edge from ca. 465 nm to 450 nm is observed for HR-CN. The corresponding band gap energy increases from 2.66 eV to 2.75 eV, implying the existence of quantum effects in HR-CN associated with incomplete

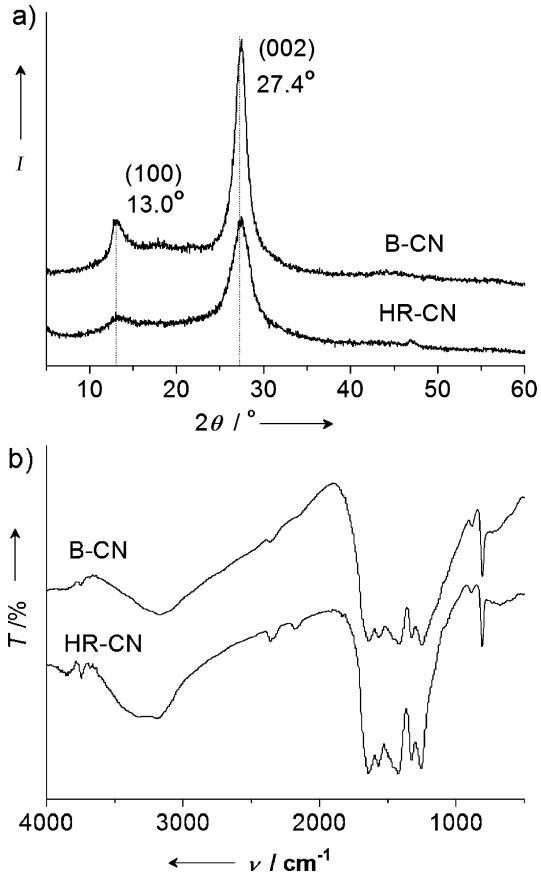

Figure 2. Structural characterization of the HR-CN sample, together with B-CN as a reference sample. a) XRD patterns and b) FTIR spectra.

condensation.[20b,21] HR-CN also displays a deeper color than B-CN due to the nanostructure effect and multiple reflections of incident light in the nanostructure (Figure S6d). A coupling of the chiral synthesis of g-C_3N_4 with the copolymerization strategy[22] to enhance the optical absorption of helical g-C_3N_4 in the visible range is feasible by fusing aromatic motifs in the g-C_3N_4 network.

The charge carriers separation/recombination rates of the samples were investigated by photoluminescence (PL) spectra at an excitation wavelength of 400 nm at room temperature, because they are key parameters in estimating the photocatalytic reactivity.[23] Broad emission peaks centering at ca. 475 nm were observed for HR-CN and B-CN because of the band–band PL phenomenon with the optical energy near the band gap energy (2.7 eV) of g-C_3N_4. Apparently, HR-CN shows lower PL intensity and stronger PL quenching than B-CN (Figure S6e). The PL quenching indeed shows a suppressed recombination rate of the photo-induced charge carriers.[23] The electronic band structure information of the sample was further tested by electron paramagnetic resonance (EPR) at room temperature (Figure S6f). Both HR-CN and B-CN exhibit one single Lorentzian line with a g value of 2.0034, which is attributed to an unpaired electron on the carbon atoms of the aromatic rings within π-bonded nanosized clusters.[12,24] Compared to B-CN, the largely stronger spin intensity of HR-CN demonstrates the promoted formation of unpaired electrons. A slightly enhanced EPR signal under visible light illumination of HR-CN provides the clue of promoted photochemical generation of radical pairs in the semiconductor.

The photoelectrochemical properties of the samples were examined by electrochemical impedance spectroscopy (EIS) (Figure S7). Nyquist plots of HR-CN in the dark exhibit remarkably decreased semicircles compared to B-CN, which suggests an enhanced electronic conductivity in the non-photoexcited state and the accelerated migration of charged carriers.[24] In addition, the photocurrent measurement was employed to investigate photoinduced electron transfer processes in carbon nitride materials casted on indium tin oxide glass. A significant enhancement of the photocurrent of HR-CN compared to that of B-CN by a factor of ten further confirms the faster transport of charged carriers in HR-CN.

The photocatalytic activities of HR-CN in hydrogen evolution, water oxidation, and CO_2-to-CO conversion were investigated. Firstly, a visible-light-induced hydrogen evolution assay was performed on HR-CN using 3 wt% Pt as the cocatalyst under visible light irradiation ($\lambda > 420$ nm) (Figure 3a and Table S1). The initial hydrogen evolution rate (HER) of HR-CN (74 μmol h^{-1}) is seven times higher than that of B-CN (10 μmol h^{-1}), and comparable to those of porous g-C_3N_4 (mpg-CN[19c] and ompg-CN[18]) having similar surface area at the same reaction conditions. Moreover, HR-CN still maintains most of its inherent photocatalytic reactivity without inactivation during the four cycles. The XRD and FTIR spectrum of HR-CN after photocatalytic reaction for 12 h remained almost unchanged (Figure S8). The TEM images of the used HR-CN display apparently unaltered twisted nanorods, except for some dark spots formed on the surface of the nanorods due to the in situ deposition of Pt nanoparticles[26] (Figure S9). These results prove the stability of the structure, texture, morphology, and reactivity of HR-CN.

We also studied the photocatalytic activity of HR-CN and 3 wt% Co_3O_4/HR-CN nanocomposites in water oxidation, using $AgNO_3$ as an electron acceptor and La_2O_3 as a pH buffer agent (Figure 3b). HR-CN exhibits a moderate oxygen evolution rate (OER) of 0.8 μmol h^{-1} under UV light ($\lambda >$ 300 nm) irradiation, whereas 3 wt% Co_3O_4/HR-CN nanocomposites show a significantly increased OER of 3.6 μmol h^{-1}, which is about four times higher than that of HR-CN. The stable evolution of O_2 and the total amount of 24 μmol O_2 in 8 h reaction were observed for 3 wt% Co_3O_4/HR-CN. Although the reactivity of HR-CN in water oxidation is not promising, the further integration of an appropriate amount of Co_3O_4 nanoparticles within HR-CN promotes its performance owing to the promoted charge separation and the reduced overpotential for water oxidation.[27]

The photocatalytic CO_2 reduction was carried out using HR-CN or B-CN as a photocatalyst, $Co(bpy)_3Cl_2$ as a redox mediator, and triethanolamine as an electron donor in acetonitrile under atmospheric CO_2 and visible light ($\lambda >$ 420 nm). Upon visible light irradiation for 1 h, the system with HR-CN photocatalyst generated CO (8.9 μmol) and H_2 (0.3 μmol) as the major gaseous products, and the catalytic turnover number relative to the amount of cobalt ions and the selectivity for CO production were calculated to be 9.2 and

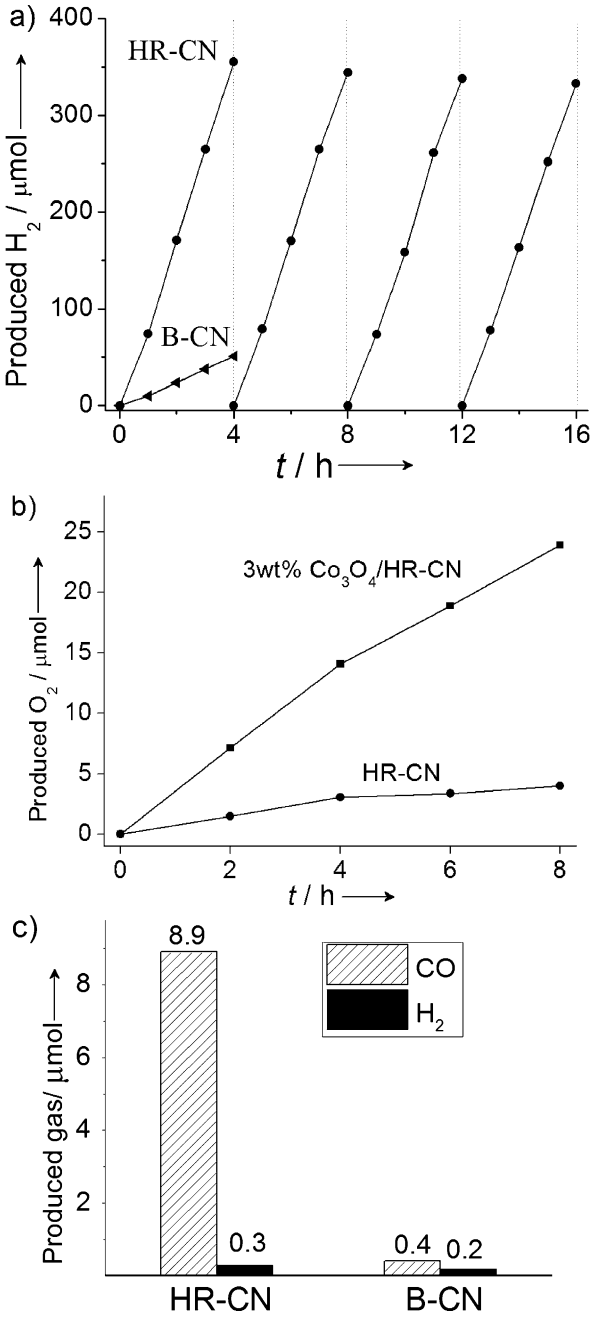

Figure 3. Photocatalytic activity of HR-CN. a) Photocatalytic H_2 evolution performance and stability test on 3 wt% Pt/HR-CN under visible light irradiation ($\lambda > 420$ nm). b) Oxygen evolution from water by HR-CN and 3 wt% Co_3O_4/HR-CN ($\lambda > 300$ nm). c) Produced gas from CO_2 reduction by HR-CN under visible light irradiation ($\lambda > 420$ nm).

96.7%, respectively (Figure 3c and entry 1, Table S2). HR-CN gives a higher yield and better selectivity for CO production than B-CN. Meanwhile, a series of reference experiments was performed. There is no detectable production of CO in the absence of either HR-CN or light (entries 3 and 4, Table S2). The evolution of CO was not observed when CO_2 was replaced with Ar gas, implying the fact that CO is not originated from the decomposition of polymeric carbon nitride or organic additives such as triethanolamine and bipyridine (entry 5, Table S2). These photocatalytic experiments indeed prove the potential application and promising prospect of HR-CN in artificial photosynthesis.

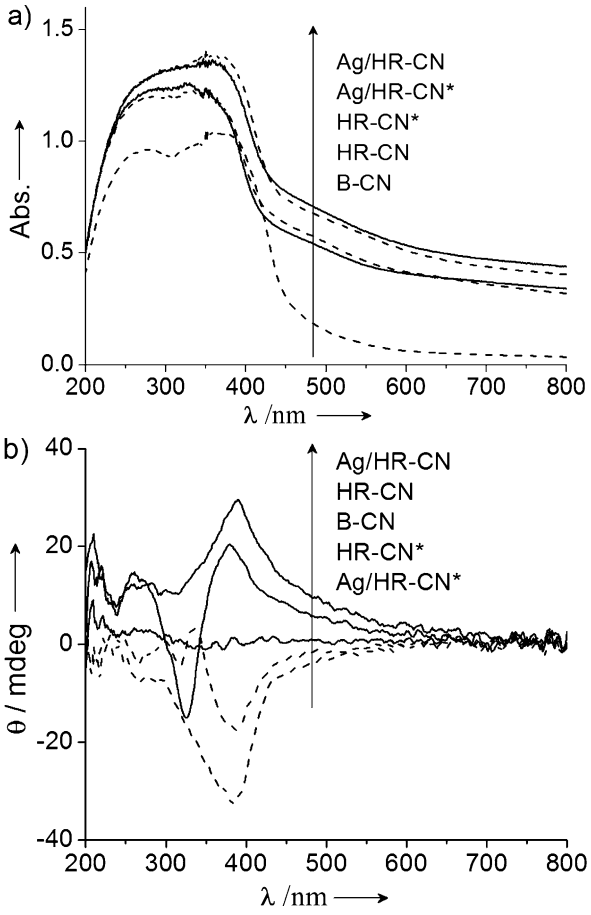

Figure 4. Optical properties and optical activities of samples. a) UV/Vis diffuse reflectance spectra. b) DRCD spectra.

Besides the photocatalytic reactivity, the helical configuration also endows the materials with distinct optical activity and chirality, which can be detected by solid-state diffuse-reflectance circular dichroism (DRCD) measurements. For reference, another helical nanorod-like g-C_3N_4 with antipodal chirality (denoted as HR-CN*) was synthesized by simply changing L-alanine into D-alanine. The UV/Vis spectra of HR-CN and HR-CN* samples (Figure 4a) similarly exhibit a broad absorption band in the range of 200–420 nm, and display stronger absorption intensity than B-CN. No obvious response was observed in DRCD spectra of B-CN (Figure 4b). Notably, the two chiral carbon nitrides with antipodal chirality show a mirror-image DRCD response in the visible region with a peak at ca. 400 nm. These DRCD results reveal that HR-CN or HR-CN* selectively reflect left- or right-handed circularly polarized light at the absorption edge. We assume that the mechanism of the optical activity for HR-CN may be similar to that of chiral TiO_2 nanofibers.[4b] The helical nanostructure of HR-CN leads to an asymmetric electric field, and the semiconductor-based electronic transitions from the valence band to the conduction band under the dissymmetric field results in its optical activity.[4b] The further loading of Ag nanoparticles on the surface of HR-CN and HR-CN* not only red-shifted the absorption edge and

enhanced the photoabsorption, but also induced stronger and more symmetrical signal in the DRCD spectra. The chiroptical properties and the mechanisms of these chirally conjugated carbon nitride materials are under investigation.

In summary, helical g-C_3N_4 rods were synthesized based on a chiral mesoporous silica template by a nanocasting method. The helical g-C_3N_4 nanorods are demonstrated to present photocatalytic capability towards hydrogen evolution, water oxidation, and CO_2-to-CO conversion. The helical-rod like g-C_3N_4 has also been shown to have unequal quantities of left- and right-handed helical nanorods and exhibits unique optical activity to circularly polarized light at the semiconductor absorption edge. It is envisaged to couple the helical structure and g-C_3N_4 photocatalysis for advanced organic photosynthesis as right- and left-handed helical silica has already been demonstrated to induce the highly enantioselective synthesis of organic compounds.[28] These chiral g-C_3N_4 materials with optical and photocatalytic activities hold great promise for optical devices, asymmetric (photo)catalysis, chiral recognition, and chiral separation.

Received: July 17, 2014
Revised: August 9, 2014
Published online: September 12, 2014

Keywords: chirality · graphitic carbon nitride · helical nanorods · optical activity · photocatalysis

[1] A. Guerrero-Martínez, J. L. Alonso-Gómez, B. Auguié, M. M. Cid, L. M. Liz-Marzán, *Nano Today* **2011**, *6*, 381 – 400.
[2] T. Aida, E. W. Meijer, S. I. Stupp, *Science* **2012**, *335*, 813 – 817.
[3] S. Liu, Y. Duan, X. Feng, J. Yang, S. Che, *Angew. Chem. Int. Ed.* **2013**, *52*, 6858 – 6862; *Angew. Chem.* **2013**, *125*, 6996 – 7000.
[4] a) P. X. Gao, Y. Ding, W. Mai, W. L. Hughes, C. Lao, Z. L. Wang, *Science* **2005**, *309*, 1700 – 1704; b) S. Liu, L. Han, Y. Duan, S. Asahina, O. Terasaki, Y. Cao, B. Liu, L. Ma, J. Zhang, S. Che, *Nat. Commun.* **2012**, *3*, 1215; c) S. Yang, L. Zhao, C. Yu, X. Zhou, J. Tang, P. Yuan, D. Chen, D. Zhao, *J. Am. Chem. Soc.* **2006**, *128*, 10460 – 10466.
[5] a) Z. Zhu, J. Guo, W. Liu, Z. Li, B. Han, W. Zhang, Z. Tang, *Angew. Chem. Int. Ed.* **2013**, *52*, 13571 – 13575; *Angew. Chem.* **2013**, *125*, 13816 – 13820; b) W. Liu, Z. Zhu, K. Deng, Z. Li, Y. Zhou, H. Qu, Y. Gao, S. Che, Z. Tang, *J. Am. Chem. Soc.* **2013**, *135*, 9659 – 9664.
[6] a) E. S. Andreiadis, M. Chavarot-Kerlidou, M. Fontecave, V. Artero, *Photochem. Photobiol.* **2011**, *87*, 946 – 964; b) A. C. Benniston, A. Harriman, *Mater. Today* **2008**, *11*, 26 – 34; c) D. Gust, T. A. Moore, A. L. Moore, *Faraday Discuss.* **2012**, *155*, 9 – 26.
[7] a) X. Wang, K. Maeda, A. Thomas, K. Takanabe, G. Xin, J. M. Carlsson, K. Domen, M. Antonietti, *Nat. Mater.* **2009**, *8*, 76 – 80; b) Y. Zhong, Z. Wang, J. Feng, S. Yan, H. Zhang, Z. Li, Z. Zou, *Appl. Surf. Sci.* **2014**, *295*, 253 – 259.
[8] a) J. Lin, Z. Pan, X. Wang, *ACS Sustainable Chem. Eng.* **2014**, *2*, 353 – 358; b) K. Maeda, K. Sekizawa, O. Ishitani, *Chem. Commun.* **2013**, *49*, 10127 – 10129; c) G. Dong, L. Zhang, *J. Mater. Chem.* **2012**, *22*, 1160 – 1166.
[9] X. Ye, Y. Cui, X. Wang, *ChemSusChem* **2014**, *7*, 738 – 742.
[10] a) B. Long, Z. Ding, X. Wang, *ChemSusChem* **2013**, *6*, 2024 – 2024; b) Y. Chen, J. Zhang, M. Zhang, X. Wang, *Chem. Sci.* **2013**, *4*, 3244 – 3248.
[11] a) J. Sun, J. Zhang, M. Zhang, M. Antonietti, X. Fu, X. Wang, *Nat. Commun.* **2012**, *3*, 1139; b) Y. Wang, X. Wang, M. Antonietti, Y. Zhang, *ChemSusChem* **2010**, *3*, 435 – 439; c) H. Yan, *Chem. Commun.* **2012**, *48*, 3430 – 3432.
[12] a) J. S. Zhang, J. H. Sun, K. Maeda, K. Domen, P. Liu, M. Antonietti, X. Z. Fu, X. C. Wang, *Energy Environ. Sci.* **2011**, *4*, 675 – 678; b) G. Liu, P. Niu, C. Sun, S. C. Smith, Z. Chen, G. Q. Lu, H. M. Cheng, *J. Am. Chem. Soc.* **2010**, *132*, 11642 – 11648; c) D. J. Martin, K. P. Qiu, S. A. Shevlin, A. D. Handoko, X. W. Chen, Z. X. Guo, J. W. Tang, *Angew. Chem. Int. Ed.* **2014**, *53*, 9240—9245; *Angew. Chem.* **2014**, *126*, 9394—9399.
[13] a) Y. Cui, Z. Ding, X. Fu, X. Wang, *Angew. Chem. Int. Ed.* **2012**, *51*, 11814 – 11818; *Angew. Chem.* **2012**, *124*, 11984 – 11988; b) M. K. Bhunia, K. Yamauchi, K. Takanabe, *Angew. Chem. Int. Ed.* **2014**, DOI: 10.1002/anie.201405161; *Angew. Chem.* **2014**, DOI: 10.1002/ange.201405161.
[14] a) P. Niu, L. Zhang, G. Liu, H. M. Cheng, *Adv. Funct. Mater.* **2012**, *22*, 4763 – 4770; b) Z. Lin, X. Wang, *Angew. Chem. Int. Ed.* **2013**, *52*, 1735 – 1738; *Angew. Chem.* **2013**, *125*, 1779 – 1782; c) K. Schwinghammer, M. B. Mesch, V. Duppel, C. Ziegler, J. Senker, B. V. Lotsch, *J. Am. Chem. Soc.* **2014**, *136*, 1730 – 1733; d) Y. Jun, J. Park, S. Lee, A. Thomas, W. Hong, G. Stucky, *Angew. Chem. Int. Ed.* **2013**, *52*, 11083 – 11087; *Angew. Chem.* **2013**, *125*, 11289 – 11293; e) M. Shalom, S. Inal, C. Fettkenhauer, D. Neher, M. Antonietti, *J. Am. Chem. Soc.* **2013**, *135*, 7118 – 7121.
[15] J. Liu, J. Huang, H. Zhou, M. Antonietti, *ACS Appl. Mater. Interfaces* **2014**, *6*, 8434 – 8440.
[16] a) H. Jin, Z. Liu, T. Ohsuna, O. Terasaki, Y. Inoue, K. Sakamoto, T. Nakanishi, K. Ariga, S. Che, *Adv. Mater.* **2006**, *18*, 593 – 596; b) H. Jin, H. Qiu, Y. Sakamoto, P. Shu, O. Terasaki, S. Che, *Chem. Eur. J.* **2008**, *14*, 6413 – 6420.
[17] S. N. Talapaneni, S. Anandan, G. P. Mane, C. Anand, D. S. Dhawale, S. Varghese, A. Mano, T. Mori, A. Vinu, *J. Mater. Chem.* **2012**, *22*, 9831 – 9840.
[18] J. Zhang, F. Guo, X. Wang, *Adv. Funct. Mater.* **2013**, *23*, 3008 – 3014.
[19] a) A. Thomas, A. Fischer, F. Goettmann, M. Antonietti, J. O. Müller, R. Schlögl, J. M. Carlsson, *J. Mater. Chem.* **2008**, *18*, 4893 – 4908; b) J. R. Holst, E. G. Gillan, *J. Am. Chem. Soc.* **2008**, *130*, 7373 – 7379; c) X. Wang, K. Maeda, X. Chen, K. Takanabe, K. Domen, Y. Hou, X. Fu, M. Antonietti, *J. Am. Chem. Soc.* **2009**, *131*, 1680 – 1681; d) J. Zhang, M. Zhang, C. Yang, X. Wang, *Adv. Mater.* **2014**, *26*, 4121 – 4126.
[20] a) J. Sehnert, K. Baerwinkel, J. Senker, *J. Phys. Chem. B* **2007**, *111*, 10671 – 10680; b) K. Kailasam, J. D. Epping, A. Thomas, S. Losse, H. Junge, *Energy Environ. Sci.* **2011**, *4*, 4668 – 4674.
[21] a) E. Z. Lee, Y. S. Jun, W. H. Hong, A. Thomas, M. M. Jin, *Angew. Chem. Int. Ed.* **2010**, *49*, 9706 – 9710; *Angew. Chem.* **2010**, *122*, 9900 – 9904; b) X. H. Li, J. Zhang, X. Chen, A. Fischer, A. Thomas, M. Antonietti, X. Wang, *Chem. Mater.* **2011**, *23*, 4344 – 4348.
[22] J. Zhang, G. Zhang, X. Chen, S. Lin, L. Möhlmann, G. Dołęga, G. Lipner, M. Antonietti, S. Blechert, X. Wang, *Angew. Chem. Int. Ed.* **2012**, *51*, 3183 – 3187; *Angew. Chem.* **2012**, *124*, 3237 – 3241.
[23] a) G. Zhang, X. Wang, *J. Catal.* **2013**, *307*, 246 – 253; b) G. Zhang, M. Zhang, X. Ye, X. Qiu, S. Lin, X. Wang, *Adv. Mater.* **2014**, *26*, 805 – 809.
[24] J. Hong, X. Xia, Y. Wang, R. Xu, *J. Mater. Chem.* **2012**, *22*, 15006 – 15012.
[25] a) M. Zhang, X. Wang, *Energy Environ. Sci.* **2014**, *7*, 1902 – 1906; b) J. Zhang, X. Chen, K. Takanabe, K. Maeda, K. Domen, J. D. Epping, X. Fu, M. Antonietti, X. Wang, *Angew. Chem. Int. Ed.* **2010**, *49*, 441 – 444; *Angew. Chem.* **2010**, *122*, 451 – 454.
[26] R. J. White, K. Tauer, M. Antonietti, M. M. Titirici, *J. Am. Chem. Soc.* **2010**, *132*, 17360 – 17363.
[27] J. Zhang, M. Grzelczak, Y. Hou, K. Maeda, K. Domen, X. Fu, M. Antonietti, X. Wang, *Chem. Sci.* **2012**, *3*, 443 – 446.
[28] I. Sato, K. Kadowaki, H. Urabe, J. H. Jung, Y. Ono, S. Shinkai, K. Soai, *Tetrahedron Lett.* **2003**, *44*, 721 – 724.

